Computer-Aided Design 45 (2013) 829–842

Contents lists available at SciVerse ScienceDirect

Computer-Aided Design

journal homepage: www.elsevier.com/locate/cad

Decomposing scanned assembly meshes based on periodicity recognition and its application to kinematic simulation modeling

Tomohiro Mizoguchi [a,*], Satoshi Kanai [b]

[a] Department of Computer Science, College of Engineering, Nihon University, 1 Nakagawara, Tokusada, Tamuramachi, Koriyama, Fukushima, 963-8642, Japan

[b] Graduate School of Information Science and Technology, Hokkaido University, Kita-14, Nishi-9, Kita-ku, Sapporo, 060-0814, Japan

ARTICLE INFO

Keywords:
X-ray CT scanning
Assembly
Periodicity recognition
Geometric synthesis
Kinematic simulation

ABSTRACT

Along with the recent growth of industrial X-ray computerized tomography (CT) scanning systems, it is now possible to non-destructively acquire the entire meshes of assemblies. This technology has the potential to realize an advanced inspection process of an assembly, such as estimation of their assembly errors or examinations of their dynamic behaviors in motion using a model reflecting real assembled situations. However, to realize the process, it is necessary to accurately decompose the mesh and to extract a set of partial meshes, each of which corresponds to a single part, from the entire meshes of assemblies measured from the CT scans. Moreover, it is required to create models that are ready for dynamic behavior simulations.

In this paper, we focus on CT scanned meshes of gear assemblies as examples, and propose beneficial methods for establishing such advanced inspections. We first propose a method that accurately decomposes the mesh into partial meshes, each of which corresponds to a single gear, using periodicity recognitions. The key idea is first to accurately recognize the periodicity of each gear, then to extract sets of topologically connected mesh elements where periodicities are valid, and finally to interpolate points in plausible ways from an engineering viewpoint to the area where surface meshes are not generated, especially the contact area between parts in the CT scanning process. We also propose a method for creating kinematic simulation models which can be used for a gear teeth contact evaluation using extracted partial meshes and their periodicities. Such an evaluation of teeth contacts is one of the most important functions in kinematic simulations of gear assemblies for predicting the power transmission efficiency, noise and vibration. The characteristics of the proposed method is that (1) it can robustly and accurately recognize periodicities from noisy scanned meshes, (2) it can estimate the plausible boundaries of neighboring parts without any previous knowledge from single-material CT scanned meshes, and (3) it can efficiently extract partial meshes from large scanned meshes containing millions of triangles in a few minutes. We demonstrate the effectiveness of our method on a variety of artificial and real CT scanned meshes.

1. Introduction

Mechanical products, especially those used in power transmission machinery, such as gear trains, bearings, ball screws, and chain sprockets, are composed as assemblies consisting of a set of parts. Since such assemblies are typically covered by housings, it is difficult to observe any assembly errors of any part or the dynamical behavior of their internal motions from outside, as shown in Fig. 1 (left). If one could capture the source of the assembly errors or the internal motions of the assemblies without any disassembling, this would enable advanced inspections which could greatly contribute to performance improvements of mechanical products.

On the other hand, industrial X-ray CT scanning systems have been developing rapidly, and it is now possible to non-destructively capture the volume model or the triangular mesh model of a whole assembly including all the parts placed inside the housings, as shown in Fig. 1 (center). However, such a model cannot be directly used for inspections of assemblies, because the portions of an individual part are not yet identified and separated. If the source of the assembly errors has to be investigated, the spatial position and orientation of each part should be identified. And if the behavior in motion has to be examined, the model of each part and their contact relations should be identified, kinematic or multi-body dynamic simulation models need to be

* Corresponding author. Tel.: +81 24 956 8748.
E-mail addresses: mizo@cs.ce.nihon-u.ac.jp (T. Mizoguchi), kanai@ssi.ist.hokudai.ac.jp (S. Kanai).

0010-4485/$ – see front matter © 2011 Elsevier Ltd. All rights reserved.
doi:10.1016/j.cad.2011.02.001

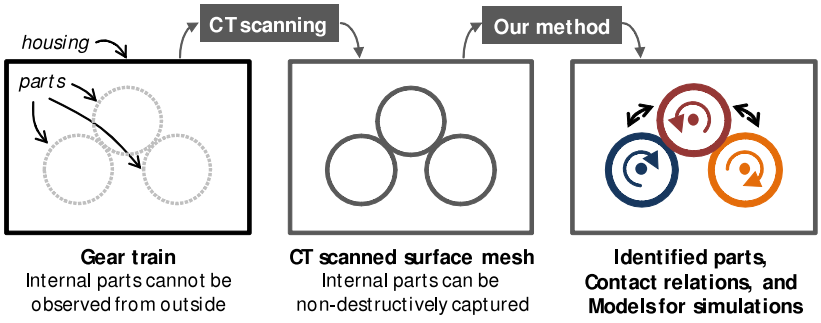

Fig. 1. An overview of our research.

created, and then the simulations must be performed. Hence, to achieve such advanced inspections of assemblies, it is necessary to extract a set of separated triangular mesh data, each of which corresponds to a single part, from their CT scanned data and to create models which can be used for estimating the assembly conditions and simulating the motions, as shown in Fig. 1 (right).

The problems become very difficult when we deal with single-material assemblies. Although the entire surface meshes of the assemblies can be acquired by the CT scan, the boundary information between parts cannot be clearly captured in the meshes. Therefore, using current methods, we cannot decompose the assembly mesh into a set of models, each of which corresponds to a single part, in straightforward way.

In this paper, we focus on the periodicities on the surfaces of assembly components, and propose beneficial methods that enable the advanced inspections of mechanical products based on periodicity recognitions. We first propose an automatic method that decomposes a CT scanned surface mesh of an assembly of parts into separated partial meshes, each of which corresponds to a single part, from a surface mesh of an assembly (subsequently referred to as "an assembly mesh") based on periodicity recognition. Our method recognizes a set of part portions having rotational periodicities from a CT scanned assembly mesh. Then, using the periodicities, the original part boundaries which cannot be captured by the CT scanning are estimated in a plausible way from an engineering viewpoint, and the assembly mesh is decomposed into separated parts along the boundaries. Our method enables the accurate decomposition of an assembly mesh composed of a single material, in which previous methods failed. And it also enables the generation of partial meshes in which some portions of the boundaries are interpolated. In addition, as an application of our mesh decomposition, we propose a new method for estimating teeth contacts of gear trains, which are the most frequently used assemblies in power transmission machineries. Our method can generate models for estimating gear assembly conditions and for performing kinematic simulations of the train, reflecting the real gear train measured by the CT scans.

We deal only with gear trains as examples in this paper, but our method is not limited to them. It can also be used for assemblies in which rotational periodicities exist in the contact area between parts, i.e., power transmissions, such as bearings and chain sprockets.

2. Related works

2.1. Periodicity recognition

Many algorithms have been proposed for recognizing periodicities in two-dimensional (2D) images. Lin et al. [1] proposed an algorithm that recognizes a translational periodicity in a 2D texture based on the generalized Hough transform. Liu et al. [2] proposed an algorithm that recognizes a variety of periodicities, including translations, rotations, and reflections, based on crystallographic theory. Müller et al. [3] proposed an algorithm for extracting a translational periodicity from a 2D façade image of a building by subdividing the image and evaluating the mutual information between the subdivided images. Musialski et al. [4] proposed an algorithm for detecting regular structures on the 2D façade images and using detected structures for repairing the images by propagating them and removing unwanted contents. However, such algorithms cannot be easily extended to 3D meshes.

Periodicity recognitions have strong relations with symmetry detections in the sense that they both find pairs of local shapes that can be closely matched to each other under certain transformation class. Recently, symmetry detections have gained much attention, and many algorithms have been proposed in the computer graphics field [5–7]. However, these algorithms aim only at detecting pairs of congruent regions and their transformations, and they cannot extract the periodicities.

As for 3D periodicity recognition, Liu et al. [8] proposed an algorithm that extracts a single region from the periodically displaced ones in a 3D mesh of a relief. However, this method requires user interactions for the extraction, and it cannot extract the parameters defining their periodicity. Pauly et al. [9] proposed an algorithm that could discover a class of periodicities defined by a combination of translations, rotations, and uniform scaling. The algorithm was based on computations of transformations under which pairs of local coordinate systems around the points can be matched, their voting to a transformation space, grid fittings in transformation space for sets of voted points, and the simultaneous registration in 3D space. However, the algorithm needs to evaluate a huge number of local transformations between a point pair for stably discovering periodicities on large and noisy scanned data; therefore, it needs a long computational time for such data. Bokeloh et al. [10] proposed an algorithm for detecting a set of congruent regions on 3D scanner data by analyzing feature lines. However, it cannot explicitly detect the parameters defining the periodicities that regions form. Zheng et al. [11] proposed an algorithm for consolidating 3D scans of buildings by detecting and utilizing large-scale repetitions. However, it requires user interactions for detecting repetitions, especially from significantly noisy, incomplete, and outlier-corrupted scans.

Li et al. [12] proposed an algorithm for detecting a wide class of approximate symmetries from B-rep CAD models by extracting characteristic points and analyzing their connectivity. The detected symmetries were then used for estimating design intents from B-rep models [13]. However, the symmetry detection algorithm proposed in [12,13] may fail to accurately detect symmetries in the case of noisy CT scanned meshes. Moreover, the method cannot explicitly compute the parameters defining the periodicities such as rotational axes, basis angles, and translational basis vectors.

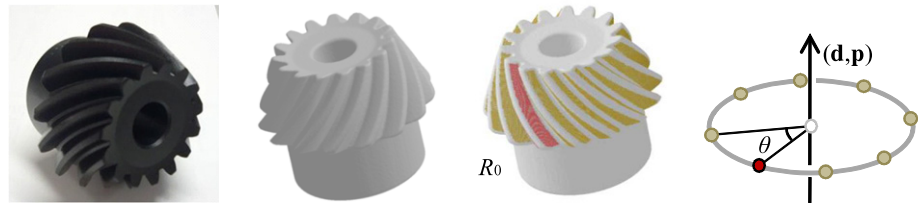

(a) Gear. (b) Scanned mesh. (c) Basis region (red). (d) Parameters defining rotational periodicity.

Fig. 2. Periodicity recognition. (For interpretation of the references to colour in this figure legend, the reader is referred to the web version of this article.)

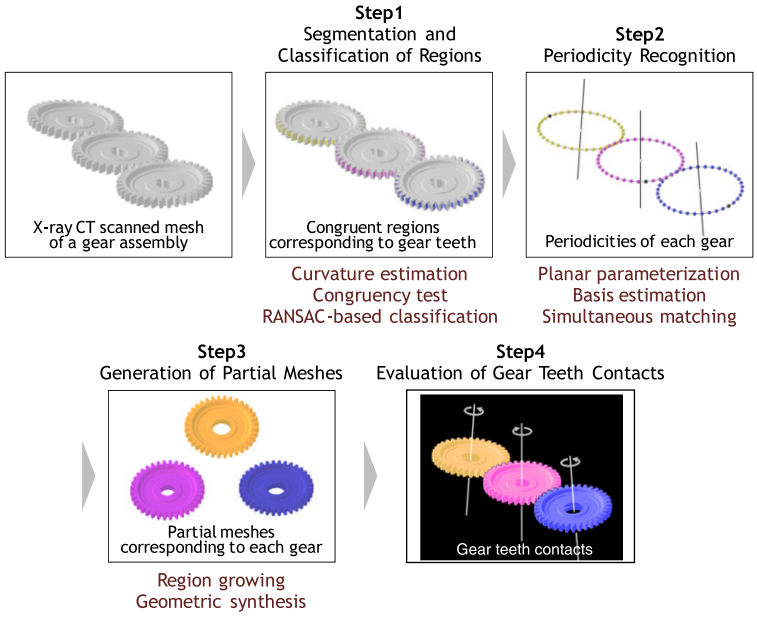

Fig. 3. An overview of our method.

2.2. Decomposition of 3D models into parts

In the computer graphics field, many mesh segmentation methods have been proposed for decomposing 3D mesh models into some meaningful portions [14,15]. These methods aim at segmenting character models such as animals into parts, i.e., heads, bodies, and legs. However, these methods find only the authentic-looking boundaries on the mesh surface, by simply finding a sequence of concave areas based on optimizations, and thus cannot estimate the correct surface boundaries between parts in an assembly mesh of engineering objects.

Alternative methods have been proposed in the digital engineering field. Shammaa et al. [16] proposed a method that registers the original CAD data corresponding to each part with CT volumetric data of part assemblies and then accurately decomposes the data into parts, each of which can be closely registered with CAD data. However, this method cannot be used when the original CAD data are not provided, for example, in the case of old products. Shammaa et al. [17] also proposed a method that decomposes the multi-material CT volumetric data into those of parts by analyzing the CT values which differ for each material, based on a graph cut. However, this method cannot be used for single-material data such as gear trains, where the CT values of every part are almost same.

3. An overview of the method

In this section, the details of our method are described by taking a gear train as an example. Usually, a 3D CAD model of a single gear can be designed first by creating a partial model including one tooth and then by rotating it around the axis by the integral multiple of the basis angle. Therefore, as shown in Fig. 2, for recognizing such a rotational periodicity from a scanned mesh, it is required to extract a basis region R_0 and a set of parameters defining the periodicity, such as an axis directional vector **d**, a point on an axis **p**, and a basis angle θ.

In this paper, we propose a new method that recognizes rotational periodicities on a CT scanned assembly mesh of a gear train and then decomposes the mesh into partial meshes, each of which corresponds to a part, based on the periodicities. In addition, as an application, we propose a method that evaluates the gear teeth contact, which is one of the most important functions in kinematic simulations, using the results of periodicity recognition and the partial meshes. As shown in Fig. 3, our method consists of following four steps.

Step 1. Segmentation and classification of regions (Section 4).

Given a CT scanned assembly mesh of a gear train generated from its CT volumetric data, the principal curvatures are estimated at each vertex based on local polynomial fittings, and vertices located around high curvature areas are detected by thresholding the estimated curvatures [18,19] (Section 4.1). Then an assembly mesh is segmented into separated regions, which are sets of topologically connected vertices, so that each region can be bounded by high-curvature vertices (Section 4.1). Next, pairwise ICP (Iterative Closest Point) matching [20] is performed to find a set of congruent regions mostly corresponding to gear teeth from the segmented regions using the fact that all teeth in a single gear have the same geometry (Section 4.2). Finally, the congruent regions are classified into groups, each of which corresponds to a single gear, based on the RANSAC-based circle fittings (Section 4.3).

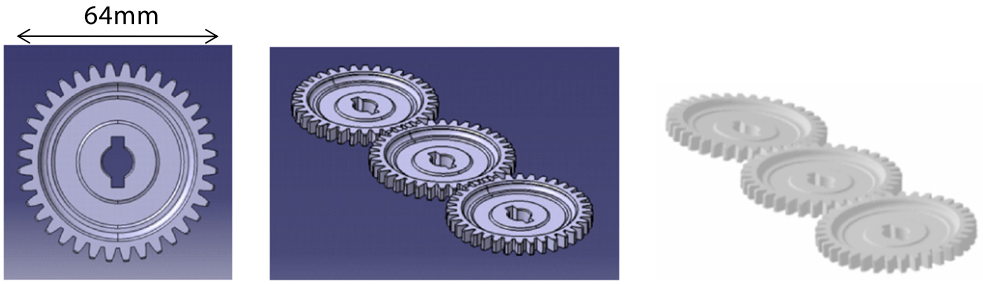

(a) CAD model of a single gear (number of teeth: 36).

(b) CAD model of gear assembly.

(c) Mesh of gear assembly (number of triangles: 447,840).

Fig. 4. An artificial mesh of a gear assembly.

Our method uses only vertices located around the region boundary for congruency tests using ICP, and it greatly reduces the computational cost without decreasing the matching accuracy.

Step 2. Periodicity recognition (Section 5).

For each group of regions, a least-squares plane is fitted to all of barycenters of the regions. Then the barycenters are projected onto the plane and their 2D parameters on the plane are calculated (Section 5.1). Then the regions in a group are classified into subgroups, each of which corresponds to one side of a gear tooth (Section 5.2). Next, for each group or each subgroup, an initial rotational axis and a basis angle are extracted based on the basis estimation method [21], and then an index that specifies the multiple of the basis angle is assigned to each region (Section 5.3). Finally, optimal parameters defining the periodicity are extracted based on our simultaneous matching algorithm [21] (Section 5.4).

Our basis estimation and simultaneous matching methods enable accurate extraction of the parameters defining the periodicities even from noisy scanned meshes such as CT scanned ones. Our method also uses only vertices around the region boundaries for the matching, so that it can greatly reduce the computational cost without decreasing the extraction accuracy.

Step 3. Generation of partial meshes (Section 6).

Extracted regions in Step 1 are then simultaneously enlarged by our region growing according to the periodicities (Section 6.1). Next, points are interpolated and filled by our geometric synthesis algorithm in the area where regions of a group are missing due to the segmentation and classification failure in Step 1 or where the surface meshes could not originally extracted from the CT scan due to the surface contact between neighboring parts. This algorithm enables us to generate all-round points of each gear to complete the individual gear shape (Section 6.2). Finally, the partial meshes, each of which corresponds to a gear, can be generated by triangulating the filled points.

Our region growing enables the extraction of as large regions as possible where periodicities are valid under the user-specified tolerance. And our geometric synthesis enables us to accurately and plausibly estimate the surface boundaries between neighboring gears and to extract and complete the meshes of each gear.

Step 4. Evaluation of gear teeth contact (Section 7).

Then pairs of partial gear meshes which contact each other are sequentially rotated around the axis by a constant pitch angle, and their teeth contacts are estimated. In our method, estimations of teeth contacts are reduced to the distance computations between smooth surfaces approximating two gear teeth regions.

Such smooth surface approximations reduce the effect of the scanning noise for the evaluations of gear teeth contacts. Moreover, our method enables us to estimate the actual gear train motion and contact behaviors based on their CT scanned surface meshes.

In the next section, the details of our method are explained using the mesh shown in Fig. 4 as an example. To generate this mesh, we first copied the CAD model of the single gear with 36 teeth in Fig. 4(a) and then created the gear train model consisting of three gears in Fig. 4(b). Then we tilted the rotational axes of the two gears by five degrees with reference to each other, and generated the gear train mesh with 447,840 triangles in Fig. 4(c) by triangulating the CAD model using the CAE meshing software. We also added artificial noise to the mesh by displacing each vertex along its normal direction by a Gaussian distributed random distance with standard deviation 5% proportional to the averaged mesh edge length.

4. Segmentation and classification of regions

4.1. Curvature estimation and segmentation

First, the principal curvatures are estimated at each vertex based on the local quadratic polynomial surface fitting [18,19], as shown in Fig. 5(a). Then, if the estimated maximum principal curvature $\kappa_{\max}$ at each vertex satisfies $1/|\kappa_{\max}| < th_{\text{high}}\, l_{\text{avg}}$, it is classified as a high-curvature vertex. As shown in Fig. 5(b), most high-curvature vertices are located in the vicinity of minute fillets or chamfers. Here, th_{high} is the threshold which must be set in a trial-and-error manner depending on the geometry and the resolutions of the mesh, and l_{avg} is the averaged mesh edge length.

Then the mesh is segmented into separated regions, each of which is a set of topologically connected vertices, bounded by high-curvature vertices, as shown in Fig. 5(c). Since the top, bottom, and sides of teeth in almost all gears include minute fillets or chamfers, and the estimated curvatures in such areas are high compared with those in interior teeth areas, our simple segmentation can correctly extract a set of regions corresponding to gear teeth separately.

We note that the similar idea is also applied for symmetry detection of man-made gears in [24].

4.2. Selection of congruent regions

Next, under the fact that all gear teeth in a single gear represent the same geometry, congruency tests are performed in all of the segmented regions $\{R_\alpha \mid 1 \le \alpha \le n_{\text{seg}}\}$ based on the pairwise ICP algorithm [20] to select a set of congruent regions mostly corresponding to the gear teeth. Here, we assume that most of the regions in the set $\{R_\alpha\}$ are congruent. The ICP algorithm matches pairs of regions so that the sum of the distances between corresponding points can be minimized. The congruent regions have the same geometry; pairs of them can be matched by the ICP algorithm, and the averaged distance between two regions in the final matched state becomes very small. However, when non-congruent regions are paired, the distance becomes large.

Based on this fact, our method applies the following procedures for selecting congruent regions.

1. The user-specified number of regions $\{Q_\beta\}$ is first selected from $\{R_\alpha\}$, and, for each Q_β, a set of pairs $\{\langle Q_\beta, R_\alpha\rangle \mid 1 \le \alpha \le n_{\text{seg}}\}$

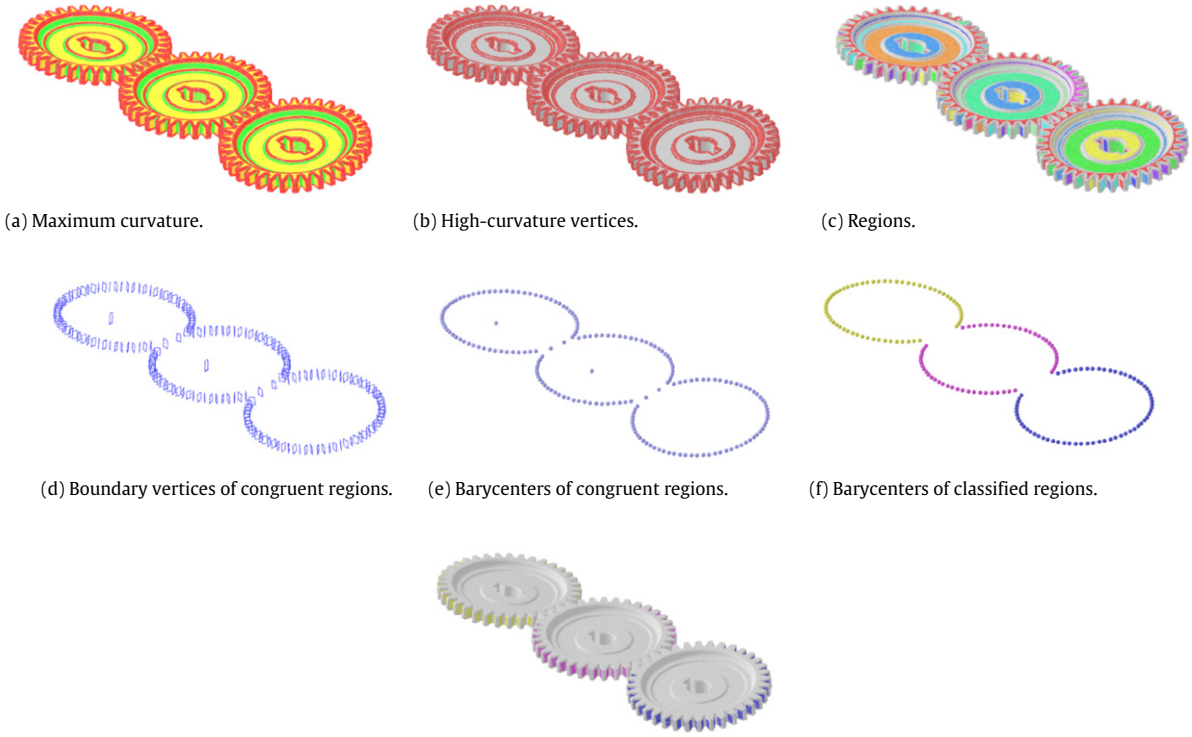

(a) Maximum curvature. (b) High-curvature vertices. (c) Regions.

(d) Boundary vertices of congruent regions. (e) Barycenters of congruent regions. (f) Barycenters of classified regions.

(g) Classified regions.

Fig. 5. Segmentation and classification of regions.

is created, where n_{seg} is the number of regions obtained by the process in Section 4.1.

2. For each pair in $\{\langle Q_\beta, R_\alpha\rangle\}$, the ICP matching is tried, and the averaged distances $\{e_{\alpha\beta}\}$ between the corresponding points is evaluated in the final matched state.
3. For each Q_β, the number of false pairs $n_{\alpha\beta}$ is counted whose $e_{\alpha\beta}$ is more than the threshold th_{cong}. We set th_{cong} so that it becomes proportional to the averaged mesh edge length l_{avg}, such that $th_{\text{cong}} = \tau_{\text{cong}} l_{\text{avg}}$. We set $\tau_{\text{cong}} = 1.0$ for all the examples in this paper.
4. If $n_{\alpha\beta} > w_{\text{cong}} n_{\text{seg}}$, Q_β is verified to be not a gear teeth region, and then we do not apply the following procedure to any $\langle Q_\beta, R_\alpha\rangle$. Otherwise, Q_β is selected as a gear teeth region, and then $e_{\alpha\beta}$ for each pair $\langle Q_\beta, R_\alpha\rangle$ is evaluated. If $e_{\alpha\beta} < th_{\text{cong}}$, R_α is finally selected as a congruent regions. We typically set $w_{\text{cong}} = 0.5$.

As a result of this process, a set of congruent regions, most of which correspond to gear teeth, can be accurately selected. As shown in Fig. 5(d), our method uses only the vertices located around the region boundaries ("boundary vertices") for ICP matching, and it greatly reduces the computational cost without decreasing the matching accuracy. We note that several regions which do not correspond to gear teeth still remain at the end of this step.

4.3. Classification of regions

Then, under the assumption that the reference points of the gear teeth of a single gear should be positioned on a circle, the barycenters of the congruent regions shown in Fig. 5(e) are classified into groups, each of which makes up a set of teeth of a single gear, based on the RANSAC-based circle fittings, as shown in Fig. 5(f). If a set of barycenters lies on one circle within a certain tolerance, they are classified into the group. This process classifies the regions into some groups $G_i = \{R_i^j\}$, as shown in Fig. 5(g). From our many experiments, we found that only the regions composing gear teeth can be picked up and grouped to an appropriate group G_i as a result of this process.

5. Periodicity recognition

5.1. Planar parameterization

Next, for each group G_i, a least-squares plane P_i is fitted for a set of barycenters $\{B_i^j\}$ of $\{R_i^j\}$. Each B_i^j is then projected onto the plane P_i and their 2D coordinates (u_i^j, v_i^j) on the plane are calculated. The axes u and v on the plane are arbitrarily defined so that they can be orthogonal to each other.

5.2. Subgrouping

As shown in Fig. 7, the gear shapes may be defined with several faces, e.g., top, bottom, and two side faces, in the CAD system. Usually, the areas of the top and the bottom faces are much smaller than those of the two side faces, and the mesh vertices corresponding to their faces tend to be classified as high-curvature vertices in Step 1. Therefore, the regions that correspond to top and bottom faces are not extracted by our segmentation, and only the two sides regions are detected.

Our current method of periodicity recognition can deal with the case where one single region or two side regions are extracted from a single gear tooth. An example of a single regions is shown in Fig. 16, and those of two side regions are shown in Figs. 5, 17 and 19–21. When the two side regions are extracted, our method separates them into two subgroups, i.e., right and left side subgroups, by the following procedures. The entire procedure is illustrated in Fig. 6.

1. For each region R_i^j, the normal vector $\mathbf{N}_i^j$ is computed as the averaged vector of the vertex normal vectors in R_i^j.

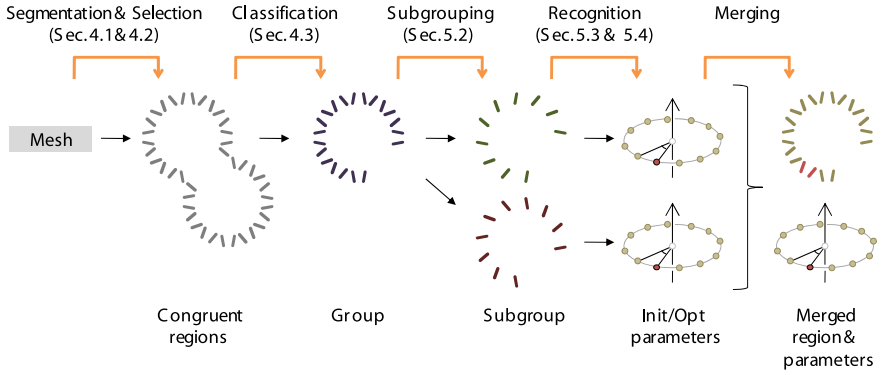

Fig. 6. Classification of regions.

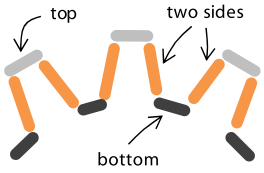

Fig. 7. Subgrouping.

2. A region R_i^x is arbitrarily selected among G_i, and the following process is applied for other regions $\{R_i^j\}$.
   2.1 The normal vector $\mathbf{N}_i^j$ is rotated by the angle between $\mathbf{B}_i^x$ and $\mathbf{B}_i^j$, and the angle $\theta_i^{x,j}$ between $\mathbf{N}_i^x$ and the rotated normal vector $\hat{\mathbf{N}}_i^j$ is estimated.
   2.2 If $\theta_i^{j,x}$ is smaller than the threshold th_{sub}, the region $R_i^j$is classified into the same subgroup as R_i^x. We set $th_{sub} = 45.0°$ for all the meshes in this paper.
3. Process 2 is repeated until there is no region which has not been classified into any subgroup.

In the following section, we describe our periodicity recognition method for each subgroup. After periodicities are recognized by the methods described in Sections 5.3 and 5.4, our method merges the subgroups into a group and obtains the merged regions and the common rotational axis and the basis angle of the group. The method is very simple and easy to implement, so we do not describe the details of it. In the next section, we refer to the subgroup as a group and denote it as $G_i = \{R_i^j\}$ for simplicity.

5.3. Initial estimation and assignment of indices

Then, for each group G_i, our method estimates the initial parameters defining the periodicity: an axis directional vector $\mathbf{d}$, a point on an axis $\mathbf{p}$, and a basis angle θ. In rotational periodicities, the projected barycenters $\tilde{B}_i^j$ are located periodically a constant angle apart on the circumference of a circle on the plane, as shown in Fig. 8. This rotational periodicity is defined by a rotational basis angle around a center of rotation. A single region R_i^j can be matched to others under a set of periodic rotations, and therefore a projected barycenter $\tilde{B}_i^j$ can also be approximately matched to others under the same rotations. Under this assumption, our method first estimates the initial parameters using the basis estimation method, which is the modification of Lin's [1]. The estimated parameters are then used to assign an index to each R_i^j.

Since we deal with CT scanned meshes, the projected barycenter coordinates include some errors caused by spatial distribution of the vertex position and by scanning noise, and they are not necessarily located at exact regular angle intervals on the circle. However, our method is a kind of voting scheme, and it can extract the best parameters from several candidates even when such positional errors are included in the barycenter coordinates. The initial parameters are estimated according to the following processes.

Estimation of the initial axis.

The estimation of the axis is easy and intuitive. It is simply computed by performing the following procedures.

1. The initial directional vector $\mathbf{d}_i^{\text{init}}$ of the rotational axis is calculated as the normal vector of the projection plane P_i.
2. A circle is fit to $\{\tilde{B}_i^j\}$, and the initial point on the axis $\mathbf{p}_i^{\text{init}}$ is estimated as the center of the circle.

Estimation of the initial basis angle.

At the beginning of this step, we regard the projected barycenters as a set of vectors $\{\tilde{\mathbf{B}}_i^j = (u_i^j, v_i^j) | \ 1 \le j \le N_i\}$ originated by $\mathbf{p}_i^{\text{init}}$. We define the basis angle as the one whose absolute value is small and whose integer multiples represent all other angles between pairs of vectors. Examples are shown in Fig. 8. If we select θ_a of Fig. 8(a) for the basis angle, the other angle θ_b cannot be represented by its integral multiple, and therefore θ_a is incorrect as a basis angle. In contrast, as in the example in Fig. 8(b), θ_a is small angle which can represent θ_b as the integral multiple of it, and therefore θ_a can be selected as a basis angle. To find such an optimal basis angle among all the angles between pairs of vectors, our method performs the following procedures.

1. A 2D accumulate array $S(j, k)$ is created, and their entries of the array are initialized as $S(j, k) = 0$ for $1 \le j, k \le N_i$.
2. For each pair of vectors $\tilde{\mathbf{B}}_i^j$ and $\tilde{\mathbf{B}}_i^k$, where $1 \le j < k \le N_i$, the following procedures are performed.
   2.1 For each vector $\tilde{\mathbf{B}}_i^l$, where $2 \le l \le N_i$, $a = \theta_b/\theta_a$ is estimated, where $\theta_a = angle(\tilde{\mathbf{B}}_i^j, \tilde{\mathbf{B}}_i^k)$ and $\theta_b = angle(\tilde{\mathbf{B}}_i^j, \tilde{\mathbf{B}}_i^l)$. And the round-off integer of a is calculated as a'.
   2.2 The value of $S(j, k)$ is updated by the scoring rule in Eq. (1).
   $$S(j, k) \leftarrow S(j, k) + \frac{1 - 2|a - a'|}{\{angle\,(\tilde{\mathbf{B}}_i^j, \tilde{\mathbf{B}}_i^k)\}^{\gamma}}. \tag{1}$$
3. The entry with the highest score in the array S is picked up as $S(\hat{j}, \hat{k})$, and then the initial basis angle θ_i^{init} is set as $angle(\tilde{\mathbf{B}}_i^{\hat{j}}, \tilde{\mathbf{B}}_i^{\hat{k}})$.

In our method, for each pair of vectors $\tilde{\mathbf{B}}_i^j$ and $\tilde{\mathbf{B}}_i^k$, as two vectors are located nearer at exact regular angle intervals on the fit circle and as their angle becomes smaller, their corresponding score $S(j, k)$ becomes higher. In Eq. (1), we set $\gamma = 0.5$ for all meshes in this paper, and we found it provided satisfactory results in various experiments.

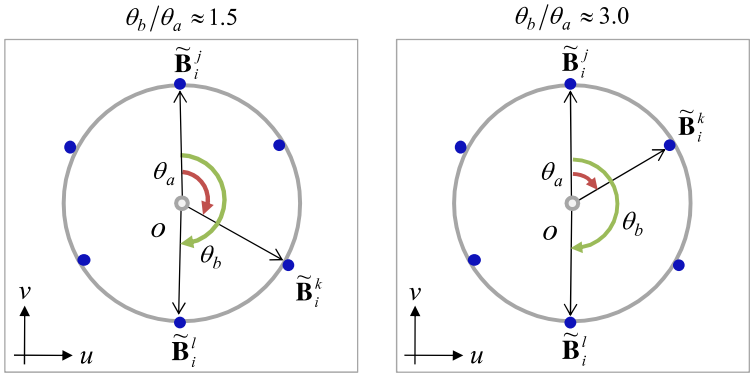

(a) Incorrect angle. (b) Correct angle.

Fig. 8. Initial estimation.

Assignment of indices.

For each vector $\tilde{\mathbf{B}}_i^j$, the value $c = \theta_c/\theta^{\text{init}}$ is evaluated, where $\theta_c = angle(\tilde{\mathbf{B}}_i^j, \tilde{\mathbf{B}}_i^1)$. Then the index of $\tilde{\mathbf{B}}_i^j$ is computed as c', where c' is the rounded-off integer of c.

5.4. Optimal estimation

In this section, we describe a simultaneous matching algorithm [21] which extracts the optimal parameters $\langle \mathbf{d}^{\text{opt}}, \mathbf{p}^{\text{opt}}, \theta^{\text{opt}} \rangle$ defining the rotational periodicities. The initial parameters calculated in Section 5.2 still include some estimation error of the rotational axis and the basis angle due to the error of calculating the projected barycenters. Therefore, this step minimizes the error by an optimization, and extracts more accurate parameters of the periodicities. Our simultaneous matching algorithm is the extension of ICP [20]. ICP iterates finding corresponding points for a pair of regions and computing a transformation to minimize the sum of squared distances between them, and it finally estimates an optimal transformation under which a pair of regions can be matched to each other so that the sum of distances between corresponding points can be minimized. In contrast to the conventional ICP, our simultaneous matching algorithm iterates finding corresponding points for all the pairs of regions and computing a rotational axis and a basis angle. It finally estimates the optimal axis and angle under which any single region can be matched to others by periodic rotations of the integer-multiplied angle about the axis so that their matching error can be minimized. More simply, our algorithm can be regarded as bidirectional distance minimization between corresponding points in all pairs of regions.

Here we denote a region R_i^j in a group G_i as a set of points $R_i^j = \{\mathbf{x}_{i,k}^j | \, 1 \le j \le N_i, \, 1 \le k \le n_i^j\}$. The point $\mathbf{x}_{i,k}^j$ can be closely matched to its corresponding point $\mathbf{x}_{i,c(k)}^l$ in the other region R_i^l by a rotation $\mathbf{T}(\mathbf{x}_{i,k}^j)$, where $\mathbf{T}(\mathbf{x}_{i,k}^j)$ is the rotation around the axis $\langle \mathbf{d}, \mathbf{p} \rangle$ with the angle $(id(R_i^j) - id(R_i^l))\theta$. Here, $id(R_i^j)$ and $id(R_i^l)$ are the indices of R_i^j and R_i^l, respectively. And $c(k)$ is the vertex number of $\mathbf{x}_{i,c(k)}^l$ closest to $\mathbf{x}_{i,k}^j$. In order to estimate the optimal rotational axis and the optimal basis angle, our algorithm performs the following procedures.

1. *Initialize*. Set $\mathbf{d}_i^0 = \mathbf{d}_i^{\text{init}}$, $\mathbf{p}_i^0 = \mathbf{p}_i^{\text{init}}$, $\theta_i^0 = \theta_i^{\text{init}}$, and itr $= 0$.
2. *Find closest points*. For each R_i^j, where $1 \le j \le N_i$, the following processes are performed.

   For each point $\mathbf{T}^{\text{itr}}(\mathbf{x}_{i,k}^j)$ in the current position of R_i^j, the set of closest point $\{\mathbf{x}_{i,c(k)}^l\}$ in each $R_i^l$is searched. And for each point $\mathbf{x}_{i,m}^l$ in the initial position of R_i^l, the set of closest point $\{\mathbf{T}^{\text{itr}}(\mathbf{x}_{i,c(m)}^j)\}$ is also searched in the current position of each R_i^j.
3. *Compute parameters*. The periodicity parameters $\langle \mathbf{d}_i^{\text{itr}}, \mathbf{p}_i^{\text{itr}}, \theta_i^{\text{itr}} \rangle$ are calculated by an optimization minimizing the sum of squared distances between corresponding points in Eq. (2):

$$D^{\text{itr}} = \sum_{j=1}^{N_i} \sum_{l=j+1}^{N_i} D^{\text{itr}}(R_i^j \to R_i^l) + \sum_{j=1}^{N_i} \sum_{l=j+1}^{N_i} D^{\text{itr}}(R_i^l \to R_i^j). \tag{2}$$

   Here, $D^{\text{itr}}(R_i^j \to R_i^l)$ and $D^{\text{itr}}(R_i^l \to R_i^j)$ are described in Eqs. (3) and (4), respectively.

$$D^{\text{itr}}(R_i^j \to R_i^l) = \sum_{k}^{n_i^j} \| \, \mathbf{T}^{\text{itr}}(\mathbf{x}_{i,k}^j) - \mathbf{x}_{i,c(k)}^l \, \|^2 \tag{3}$$

$$D^{\text{itr}}(R_i^l \to R_i^j) = \sum_{m}^{n_i^l} \| \, \mathbf{x}_{i,m}^l - \mathbf{T}^{\text{itr}}(\mathbf{x}_{i,c(m)}^j) \, \|^2. \tag{4}$$

   This nonlinear equation can be solved for $\mathbf{d}_i^{\text{itr}}$, $\mathbf{p}_i^{\text{itr}}$, and θ_i^{itr} using the Levenberg–Marquardt algorithm.
4. *Update points and calculate distance*. The points are calculated such that $\mathbf{T}^{\text{itr}}(\mathbf{x}_{i,k}^j) \leftarrow \mathbf{x}_{i,k}^j$ using the current parameters $\mathbf{d}_i^{\text{itr}}$, $\mathbf{c}_i^{\text{itr}}$, and θ_i^{itr}. Then the averaged distance is also calculated using Eq. (2) as $E^{\text{itr}} = \sqrt{D^{\text{itr}}}/N_i^{\text{all}}$, where N_i^{all} is the total number of pairs of corresponding points in group G_i.
5. *Termination condition*. If $E_i^{\text{itr}} - E_i^{\text{itr}+1} > \varepsilon$, update itr $\leftarrow$ itr $+ 1$ and repeat the process from Step 2. Otherwise, the optimal parameters are output as $\mathbf{d}_i^{\text{opt}} = \mathbf{d}_i^{\text{itr}}$, $\mathbf{p}_i^{\text{opt}} = \mathbf{p}_i^{\text{itr}}$, and $\theta_i^{\text{opt}} = \theta_i^{\text{itr}}$, and then the process is terminated. In this study, we set ε such that $\varepsilon = w_{\text{opt}} l_{\text{avg}}$, typically with $w_{\text{opt}} = 0.001$.

6. Generation of partial meshes

For the purpose of inspecting the assembly errors of gear trains, the methods mentioned in the previous section are sufficient where the rotational axes are estimated. However, for performing kinematic simulations based on their CT scanned meshes, the meshes obtained from the periodicity recognition are still insufficient, because several gear teeth portions are missing in the mesh at the gear-to-gear contact area. A set of complete meshes, each of which expresses a closed surface of an individual gear, must be modeled in the simulation of gear teeth contacts. To generate such a complete mesh of each gear, our method first enlarges the gear teeth regions and extracts as large regions as possible where periodicities are valid by our simultaneous region growing. Then our geometric synthesis fills the additional points onto the false regions where the appropriate gear teeth regions are not detected by our segmentation and classification (mentioned in Section 4) and where surface meshes are not created in the CT

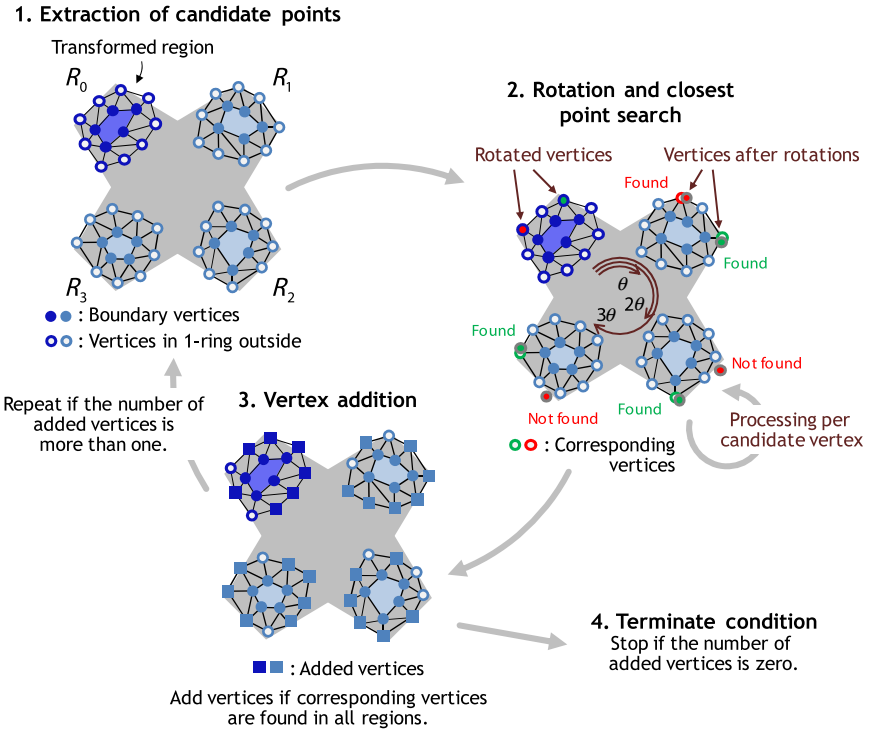

Fig. 9. An overview of our region growing.

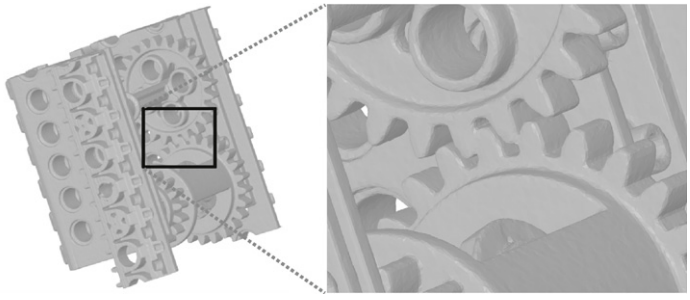

Fig. 10. Connected area on meshes due to the blur of CT values.

scanned mesh. These procedures can extract the enlarged and the synthesized all-round point sets for each gear, and the complete meshes of the gears can be created by triangulating them.

6.1. Region growing

For each group $G_i = \{R_i^j\}$, the regions extracted in Step 1 are simultaneously enlarged by our region growing algorithm according to the estimated periodicity. Since we deal with scanned meshes, the mesh vertices of each congruent region do not lie in an identical position. Therefore, our region growing allows a user-specified tolerance, and enables the extraction of as large regions as possible where periodicities are valid under the tolerance. As shown in Fig. 9, this region growing performs the following procedures.

1. *Extraction of candidate points.* A set of candidate points $C_i^j = \{\mathbf{x}_{i,k}^j\}$ is extracted as the candidates to be added to the original regions. Here, C_i^j includes vertices which lie on the boundaries of the current region and vertices which lie outside of it among their 1-ring vertices.
2. *Rotation and closest point search.* Each vertex $\mathbf{x}_{i,k}^1$ in C_i^1 is transformed to $\{\mathbf{x}_{i,k}^{1\to j}\}$ by rotating it by an angle $(id(R_i^j) - id(R_i^1))\theta_i^{\text{opt}}$ so that C_i^1 can be matched to each C_i^j. Then, for each point $\mathbf{x}_{i,k}^{1\to j}$, a set of closest points $\{\mathbf{x}_{i,c(k)}^j\}$ in each C_i^j is searched, and the distances $\{d_{i,k}^{1,j}\}$ between them are evaluated.
3. *Vertex addition.* If all the distances $\{d_{i,k}^{1,j}\}$ are less than threshold th_{add}, then $\mathbf{x}_{i,k}^1$ is added to R_i^1 and $\{\mathbf{x}_{i,c(k)}^j\}$ to $\{R_i^j\}$, respectively. We typically set $th_{\text{add}} = 1.0l_{\text{avg}}$.
4. *Terminate condition.* If the number of points added to R_i^1 is more than one, the process continues from process 1. Otherwise, stop the process.

As a result of the process, regions can be enlarged, as shown in Fig. 12(a). In Fig. 12, regions are colored according to their indices, i.e., light for odd and dark for even indices.

6.2. Geometric synthesis

When pairs of teeth in gears are in contact or very close to each other in the CT scanning process, these areas on meshes are connected, and their exact boundaries cannot be measured, as shown in Fig. 10, due to the blur of CT values. Our segmentation and congruency tests in Step 1 cannot extract the mesh of gear teeth regions around these contact areas. Moreover, even when

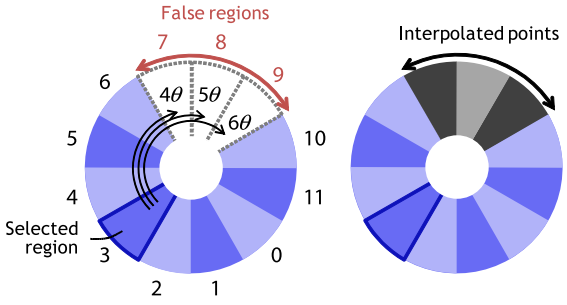

Fig. 11. Geometric synthesis.

the meshes are appropriately created, our segmentation may fail to extract regions due to inadequate threshold setting, especially when the number of vertices in the regions is small. In addition, even when our segmentation is successful, our classification method may fail to appropriately classify regions into a group due to the large positional error of the regions' barycenters. In these cases, it results that there exist several false regions after the simultaneous region growing mentioned in Section 6.1, as shown in Figs. 12(a), 16(c), (f), and 17(c). Therefore our geometric synthesis interpolates points in such areas and plausibly estimates the original geometry.

In our method, an arbitrarily selected region R_i^j is transformed to the false region $R_i^l = \{\}$ by rotating it by $(id(R_i^j) - id(R_i^l))\theta^{\text{opt}}$, and points are interpolated, as shown in Figs. 11 and 12(b). This enables us to generate all-round points for each gear to complete the gear geometry, and then meshes $\{M_i\}$ of each part without missing portions can be easily generated by triangulating them, as shown in Fig. 12(c). We are currently using the commercial software Geomagic [23] for this triangulation, but existing meshing algorithms such as marching cubes [22] can also be used.

We note that our method cannot regenerate the exactly correct boundaries of the gears but can find the boundaries where periodicities are valid. However, such boundaries are sufficient for the kinematic simulation purposes.

7. Evaluation of gear teeth contacts

In this section, a method is described for evaluating gear teeth contacts using the extracted periodicities and the partial meshes. Such an evaluation is one of the most important functions in kinematic simulations of gear assemblies for predicting the power transmission efficiency, noise, and vibration. In our method, evaluations of gear teeth contacts are replaced by the distance computations between surfaces approximating the teeth region geometries. More precisely, our method rotates the pair of partial meshes of two teeth meeting each other around each axis by a specified pitch angle, and computes the distances between the approximating surface of one tooth and the vertices projected onto the surface approximating the other one at each rotation angle. The smooth surface approximations can decrease the effect of scanning noise for the contact evaluations. We are currently using bicubic

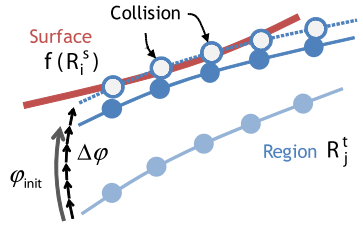

Fig. 13. Initial matching.

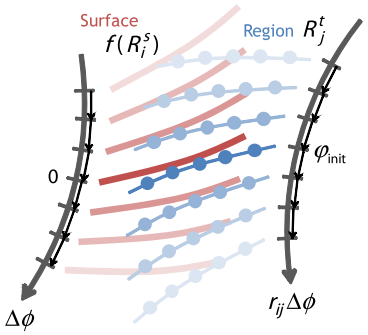

Fig. 14. Evaluation of gear teeth contacts.

polynomial surfaces for the approximation so that they can be closely fitted for a larger class of teeth faces. Our method performs the following procedures.

1. *Extraction of pairs of partial gear meshes*. The pairs of partial gear meshes $\langle M_i, M_j\rangle$ meeting each other are extracted by simply thresholding the shortest distance between pairs of approximating surfaces of the teeth.
2. *Computation of pitch angle ratio*. For each pair $\langle M_i, M_j\rangle$, the pitch angle $\langle\phi_i, \phi_j\rangle$ is calculated as $\phi_i = 360/L_i$ and $\phi_j = 360/L_j$, respectively, where L_i and L_j are the numbers of teeth in each gear. The ratio $r_{ij} = \phi_j/\phi_i$ is also computed.
3. *Initial matching*. For each pair $\langle M_i, M_j\rangle$, the pair of regions $\langle R_i^s, R_j^t\rangle$ corresponding to a pair of gear teeth which are almost in contact is found. Then the initial matching can be performed so that the pair can be almost in contact. First, a bicubic polynomial surface $f(R_i^s)$ is fitted to R_i^s in a least-squares manner. Next, as shown in Fig. 13, R_j^t is sequentially rotated by a specified pitch angle $\Delta\varphi$, the collision is tested between $f(R_i^s)$ and R_j^t, and the adjacent angle φ_{init} is detected before their collision. Then the initial matching can be performed by rotating M_j by the computed angle θ_{init} such that $M_j \to M_j'$. We set $\Delta\varphi = 0.01°$ for the example in Fig. 18. To enable performing the initial matching more accurately, we have to generate more points on the surface $f(R_i^t)$ and to make $\Delta\varphi$ smaller.
4. *Evaluation of teeth contacts*. M_i and M_j' are rotated by the pitch angle $\Delta\phi$ and $r_{ij}\Delta\phi$, respectively, and the contact is evaluated as the distance between the surface $f(R_i^s)$ and the region $R_j'^t$ which are in contact at each rotation, as shown in Fig. 14. We set $\Delta\phi = 0.1°$ for the example in Fig. 18.

(a) Grown regions. (b) Interpolated points. (c) Partial meshes.

Fig. 12. Generation of partial meshes.

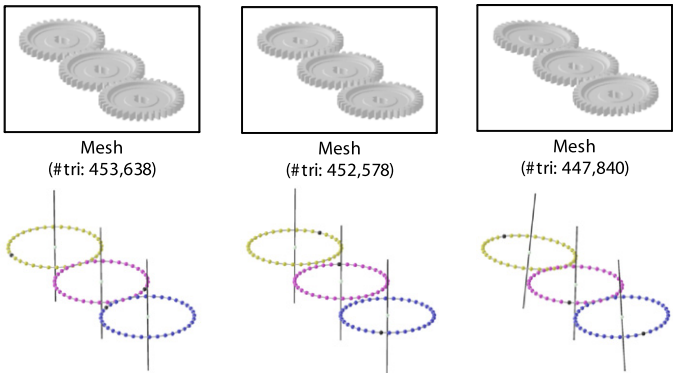

(a) Normal type. (b) Floating type. (c) Tilting type.

Fig. 15. Gear teeth recognition results from artificial assembly meshes.

Table 1
Accuracy evaluation of periodicity parameter extraction.

	Normal-type			Floating-type			Tilting-type		
Noise level (a%)	5.0	10.0	15.0	5.0	10.0	15.0	5.0	10.0	15.0
Maximum direction error (degree)	0.19	0.05	0.45	0.15	0.02	0.21	0.05	0.02	0.29
Maximum basis angle error (degree)	0.01	0.01	0.01	0.01	0.01	0.01	0.01	0.01	0.01

8. Results

We applied the proposed method for various meshes of simple gear trains and verified its effectiveness. The experiments were run on a PC with Xenon 2.0 GHz CPU and 8 GB RAM for the mesh in Fig. 19 and on a PC with Core2Duo 2.4 GHz CPU and 2 GB RAM for other meshes.

Fig. 15 shows the results of periodicity recognitions for the artificial assembly meshes of gear trains. These three types of mesh, (a)–(c), were generated in a similar way by triangulating a CAD model of the gear assembly in Fig. 4 and by generating meshes using CAE software. The first assembly mesh (Fig. 15(a)) is a normal-type one, and it does not have any assembly error. The second mesh (Fig. 15(b)) is a floating-type one, generated first by translating two gear models along the rotational axis by 6 and 3 mm with reference to one of three gears, which imitates positional offset errors along the axis between gears. The third mesh (Fig. 15(c)) is a tilting-type one, generated first by rotating two gear models by ten and five degrees with reference to one of three gears, which imitates the axis misalignments between gears. The assembly meshes contain about 450,000 triangles. We added artificial noise to the meshes by displacing each vertex along its normal direction by Gaussian distributed random distances with the standard deviation α% proportional to the averaged mesh edge length.

We set $\alpha = 5.0, 10.0, 15.0$, and evaluated the accuracy of extracting the periodicity parameters from the three types of assembly mesh at the three settings. Our method could extract the periodicities whose region barycenters are shown in Fig. 15 from all meshes at any noise level settings. We compared the axis direction and the basis angle extracted from the three types with their theoretical values. The results are shown in Table 1. The maximum error of axis direction among the three gears was 0.45° in the case of normal-type mesh with $\alpha = 15.0$. The errors of basis angles were less than 0.01° in all cases. The average number of vertices of the gear teeth regions was about 90, and the total running time for the recognitions was about 70 s.

Fig. 16 shows the results of the periodicity recognition and the partial mesh generation from a CT scanned mesh of the crankshaft sprocket gear shown in Fig. 16(a). We interactively extracted the gear portion mesh shown in the orange box from a CT scanned assembly mesh of a crankshaft. Assuming that some sprocket gear teeth contacts with a chain and that the surface meshes of these contact portions cannot be properly created, we manually cut off one and two portions of the gear teeth, as shown in Fig. 16(b) and (e). In this sprocket example, the estimation error of the basis angles was less than 0.01° with reference to the theoretical angle in both meshes. This result shows that our method can accurately recognize periodicities even when segmentation cannot be appropriately performed. Moreover, it could regenerate all-round partial meshes from such incomplete meshes using the proposed geometric synthesis, as shown in Fig. 16(d) and (g). We set the threshold th_{high} for classifying high-curvature vertices (mentioned in Section 4.1) as $th_{\text{high}} = 3.0$, and the running time was less than 2 s for both meshes.

Fig. 17 shows the results for the decomposition of the CT scanned mesh of a LEGO gear train. The train includes six gears, but only three of them could be extracted by our method. For the detected three gears, our method could interpolate the points even when regions cannot be appropriately extracted in Step 1, as shown in Fig. 17(c), and it generated the partial meshes in Fig. 17(d). In this example, the estimation errors of the basis angle were less than 0.01° in all gears. The mesh includes 981,036 triangles. The running time was 261 s in Step 1, 6 s in Step 2, and 3 s in Step 3, except for mesh generations from interpolated points. We note that most of the time in Step 1 was spent on the congruency test based on pairwise ICP matching as in [9]. As shown in Fig. 17(b), since many regions which are not gear teeth still remained after congruency tests based on ICP matching, the RANSAC algorithm could not classify three of the six gear teeth regions. We set $th_{\text{high}} = 10.0$ for this mesh.

Fig. 18 shows the results for the evaluation of gear teeth contacts for the pair of meshes M1 and M2 in Fig. 17(d) obtained from the assembly mesh of 17(a). In this figure, the contacts of the pair of teeth at several rotation angles starting from an angle φ_x are shown. Red corresponds to larger distance and yellow to zero. In the case of spur gears, as shown in this figure, if the rotational axes of the pair of gears are parallel, the tooth contact area should be a straight line parallel to the axes, and the line moves from the root to the head of the teeth. As shown in Fig. 18, the motion behaviors of the real gear assembly could be estimated even from their CT scanned meshes by our method. We also observed similar

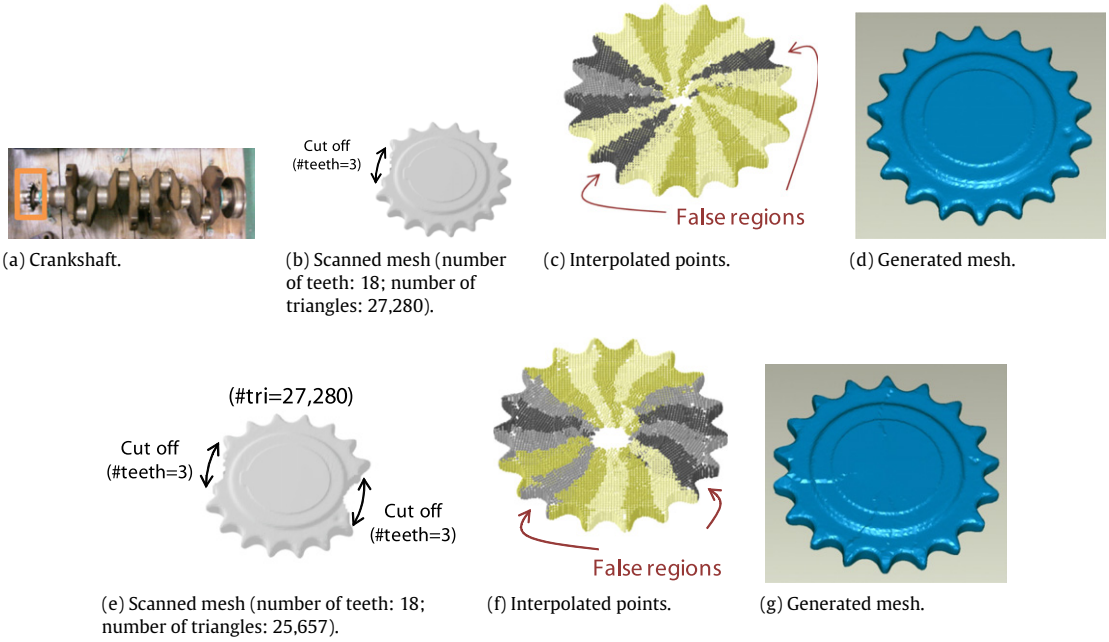

(a) Crankshaft. (b) Scanned mesh (number of teeth: 18; number of triangles: 27,280). (c) Interpolated points. (d) Generated mesh.

(e) Scanned mesh (number of teeth: 18; number of triangles: 25,657). (f) Interpolated points. (g) Generated mesh.

Fig. 16. Results for CT scanned meshes of the gear in a crankshaft.

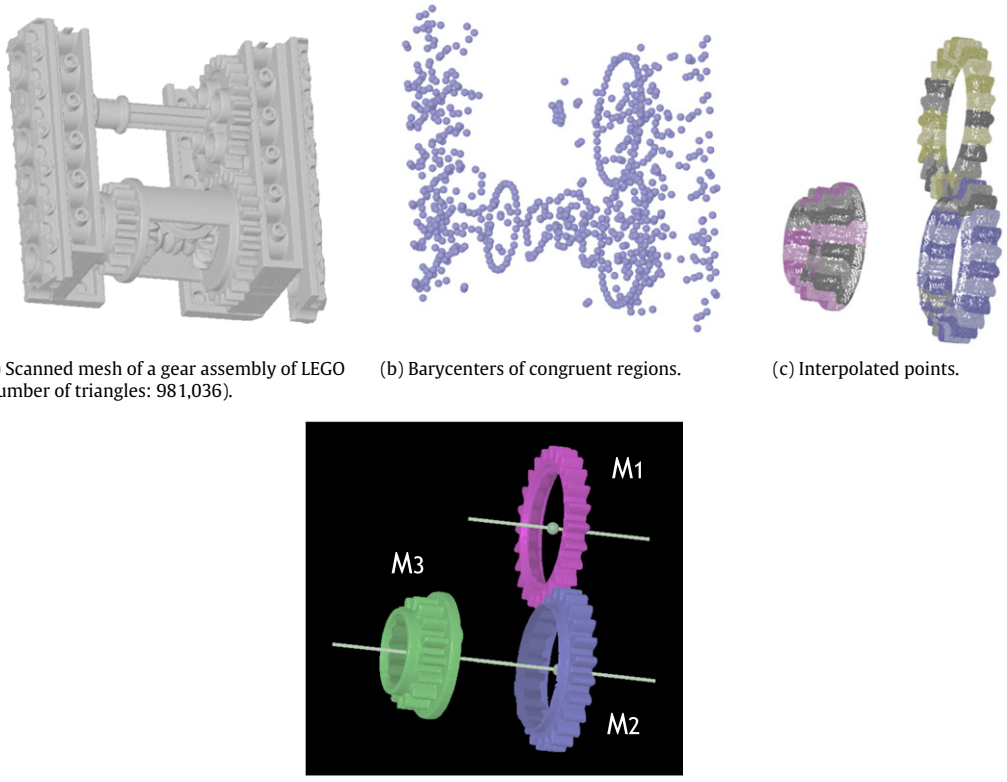

(a) Scanned mesh of a gear assembly of LEGO (number of triangles: 981,036). (b) Barycenters of congruent regions. (c) Interpolated points.

(d) Extracted partial meshes.

Fig. 17. Results for a generation of partial meshes from a CT scanned mesh.

behaviors from other pairs. The total running time was about 10 s for this pair.

Fig. 19 shows the results for the decomposition of the large CT scanned mesh including 9,062,260 triangles of the plastic gear assembly. It includes four spur gears, and three of them were double gears. Our method recognized all of four gears by analyzing the barycenters of the congruent regions in Fig. 19(b), and it regenerated the all-round point sets, as shown in Fig. 19(c), using periodicity recognition and geometric synthesis. As for each double gear, our method recognized the larger and the smaller gears separately; therefore, we manually combined them into a single mesh, as shown in Fig. 19(d). For the detected gears, the maximum estimation error of the basis angle was 0.015° in the case of the gear shown in red in Fig. 19(c), and the others were all less than

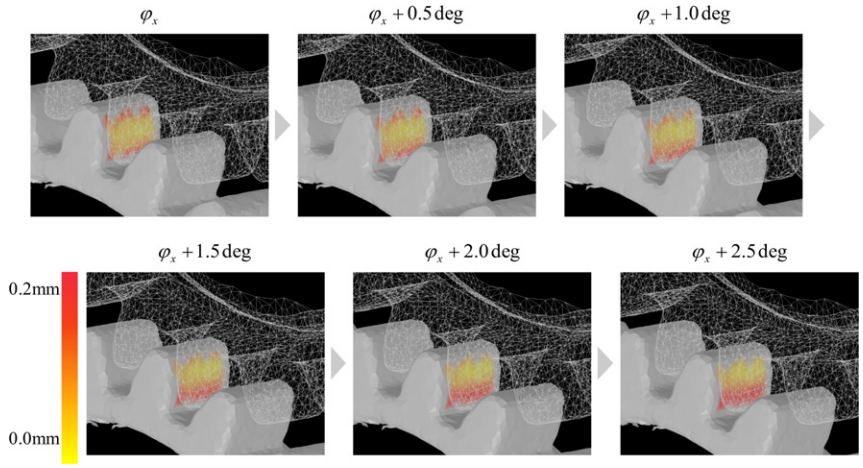

Fig. 18. Result for evaluating gear teeth contacts.

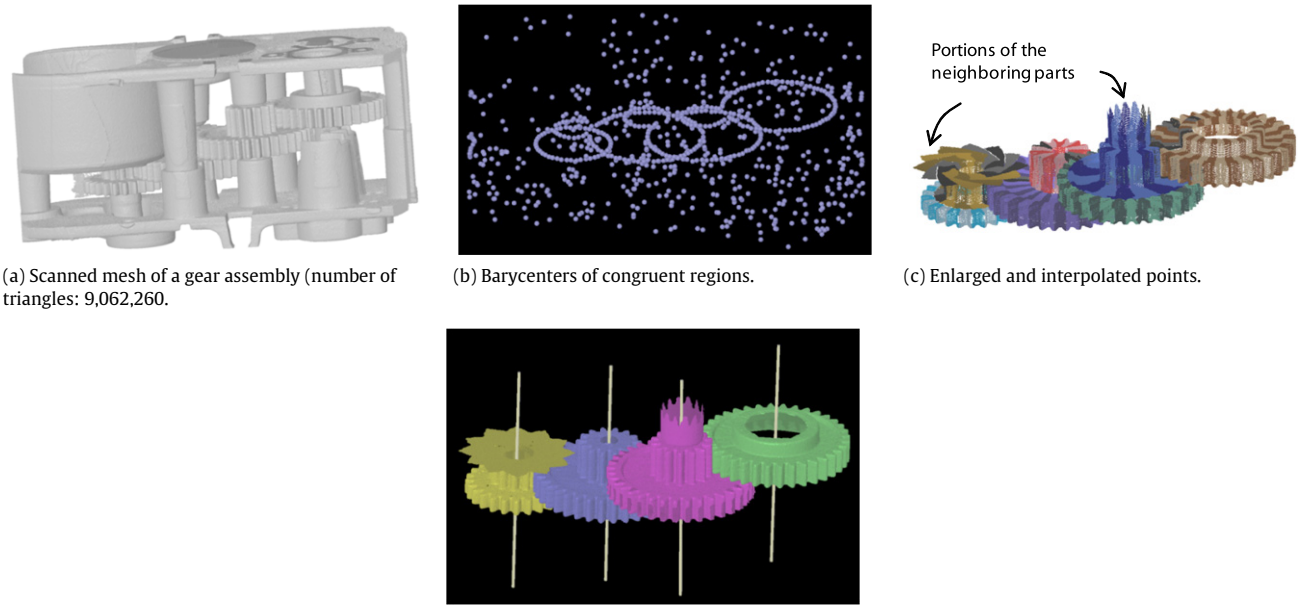

(a) Scanned mesh of a gear assembly (number of triangles: 9,062,260.

(b) Barycenters of congruent regions.

(c) Enlarged and interpolated points.

d) Extracted partial meshes and rotational axes.

Fig. 19. Results for a generation of partial meshes from a large CT scanned mesh.

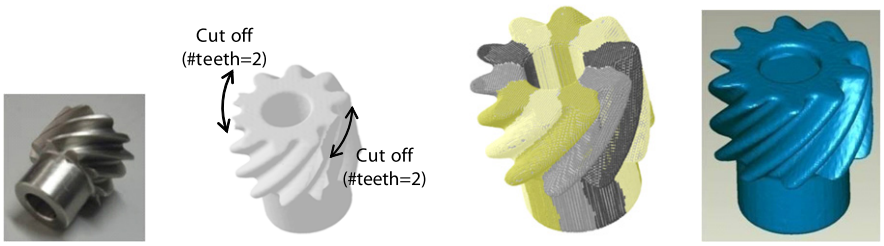

(a) Gear.

(b) Scanned mesh (number of teeth: 10; number of triangles: 106,227).

(c) Interpolated points.

(d) Generated mesh.

Fig. 20. Result for the all-round mesh generation from a CT scanned mesh of a gear.

0.01°. The running time was 486 s in Step 1, 102 s in Step 2, 373 s in Step 3, except for mesh generations from interpolated points, and 961 s in total.

As shown in Fig. 19(b), since only a few regions which did not correspond to gear teeth remained after congruency tests and the seven circles fitted to each gear were clear, the proposed algorithm worked well, and it could generate the partial meshes of each gear. We set $th_{\mathrm{high}} = 10.0$ for this mesh. Although several portions of the neighboring parts are also recognized as parts of the gears as shown in Fig. 19(c) and (d), kinematic simulation can be satisfactorily performed by using them. We note that we removed a motor and two shaft parts mostly made of aluminum from the

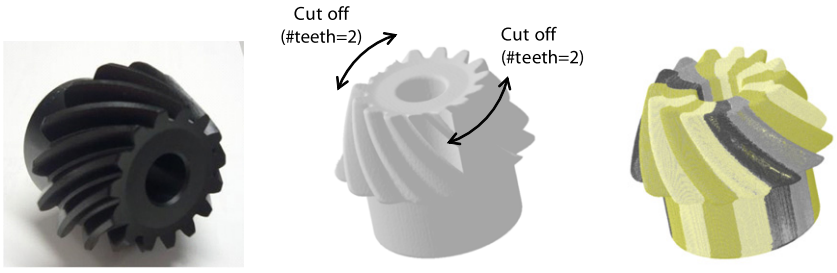

(a) Gear. (b) Scanned mesh (number of teeth: 15; number of triangles: 301,924). (c) Interpolated points.

Fig. 21. Result for the all-round points generation from a CT scanned mesh of an engineering object.

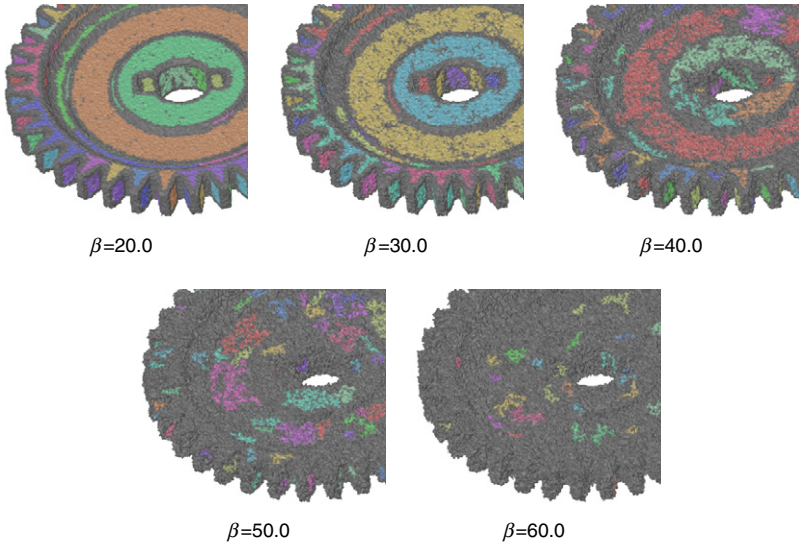

Fig. 22. Evaluation of our curvature based segmentation for noisy meshes.

assembly before the CT scanning process, since the appropriate CT threshold value for separating the aluminum from the plastic parts could not be found.

Figs. 20 and 21 show the results of periodicity recognition and partial mesh generation for bevel gears. In both figures, some portions of the mesh were manually cut off in a same way as the meshes in Fig. 16. These results show that our proposed processes could be applied for the various types of CT scanned meshes of real gears, and that it could well generate the all-round surface meshes. Therefore, it is highly probable that our whole algorithm still works well for real CT data of real gear trains. We set $th_{\text{high}} = 10.0$ for all meshes in Figs. 19 and 20.

For evaluating how much noise our curvature based segmentation methods can handle, we added the artificial noise to the mesh in Fig. 4 using the same way with standard deviation β% and tested our segmentation. The results are shown in Fig. 22. All the gear teeth are appropriately segmented up to $\beta = 20.0$. However, the number of segmented regions got smaller and the congruency of them are lost with increasing value of β.

Discussions. Our segmentation algorithm mentioned in Section 4 may fail to extract regions corresponding to gear teeth due to the scanning noise and to inappropriate threshold setting for the classification of high-curvature vertices. Moreover, it cannot detect regions of gear teeth which are in contact in the CT scanning process. In addition, our classification algorithm based on RANSAC-based circle fittings may fail to classify the regions into groups, each of which corresponds to a single gear, due to the positional error of the barycenters of the regions. Even in such cases, our periodicity recognition and partial mesh generation algorithms can recover such false regions and reconstruct the complete meshes. Examples are shown in Figs. 16 and 17. In these figures, although several regions are not correctly segmented or classified, our method could regenerate the complete meshes which can be used for kinematic simulations. In our experiments, our algorithm can generate the complete meshes when about half the regions are correctly segmented and classified. We note that the extraction accuracy of parameters, such as rotational axes and basis angles, decreases as fewer regions are segmented and are classified.

Limitations. In some gears, the surface area of a tooth is very small, and therefore the number of vertices in such regions in a scanned mesh also becomes small. In this case, our segmentation cannot appropriately extract these teeth regions due to the difficulties in setting the threshold, and thus it cannot generate partial meshes of such gears, as shown in Fig. 17.

As for the practical evaluations of gear teeth contacts in the mechanical engineering sense, more precise evaluations are required, e.g., of order a few microns or less, but the current resolution of CT scanning is not necessarily sufficient for such precise evaluations. However, the resolution of CT scanning is likely to be enhanced in the near future, and our method can then be used.

9. Conclusion and future works

In this paper, we have proposed a new method for decomposing CT scanned assembly meshes of part assemblies based on periodicity recognition. We demonstrated the effectiveness of our method from various experiments on artificial and the CT scanned meshes. By taking gear trains as examples, we verified

that our method enabled us to uniquely determine the correct boundaries between parts and to accurately decompose surface meshes composed of a single material into partial meshes, each of which corresponds to a single gear, without reference data such as original CAD data and CT threshold values. Moreover, we proposed a method for evaluating gear teeth contacts by using the generated partial meshes and the recognized periodicities as an example of kinematic simulations. We found that our method could estimate the behaviors of gear train motion based on their CT scanned assembly meshes.

Our proposed method can be used not only for gear trains as presented in this paper but also for a wide class of assemblies where rotational periodicities exist in the contact area between parts, e.g., bearings and chain sprockets. We will test the versatility of our method for such assemblies in the future.

Acknowledgements

We thank Ichiro Nishigaki and Noriyuki Sadaoka of HITACHI Co. Ltd for motivating us toward this research topic and providing the CT scanned meshes of the engineering parts in Figs. 2, 16, 20 and 21, Hiroyuki Tanaka and Hideaki Aiyama of Hokkaido Industrial Research Institute for providing the CT scanned mesh of the LEGO block in Figs. 10, 17 and 18, and Masayasu Hashimoto of Fukushima Technology Center for his useful comments and for providing the CT scanned mesh of the gear assembly in Fig. 19. We also thank Takashi Michikawa of the University of Tokyo for providing us with the surface mesh generation software from CT volumetric data. This work was financially supported by a Grant-in-Aid for Scientific Research under project No. 18004488-00 and Dean's Grant for Specified Incentive Research, College of Engineering, Nihon University.

References

[1] Lin HC, Wang LL, Yang SN. Extracting periodicity of a regular texture based on autocorrelation functions. Pattern Recognition Letters 1997;18:433–43.
[2] Liu Y, Collins TT, Tsin Y. A computational model for pattern perception based on frieze and wallpaper groups. IEEE Transactions on Pattern Analysis and Machine Intelligence 2006;26(3):354–71.
[3] Müller P, Zeng G, Wonka P, Gool LV. Image-based procedural modeling of facades. ACM Transactions on Graphics 2007;26(3):85.
[4] Musialski P, Wonka P, Recheis M, Maierhofer S. Symmetry-based Façade repair. In: Proc. vision, modeling, and visualization workshop. 2009.
[5] Mitra NJ, Guibas LJ, Pauly M. Partial and approximate symmetry detection for 3D geometry. ACM Transactions on Graphics 2006;25(3):560–8.
[6] Podolak J, Shilane P, Golovinskiy A, Rusinkiewicz S, Funkhouser T. A planar-reflective symmetry transform for 3D shapes. ACM Transactions on Graphics 2006;25(3):549–59.
[7] Xu K, Zhang H, Tagliasacchi A, Liu L, Li G, Meng M, Xiong Y. Partial intrinsic reflectional symmetry of 3D shapes. ACM Transactions on Graphics (SIGGRAPH Asia 2009) 2009;28(5). Article No.138.
[8] Liu S, Martin RR, Langbein FC, Rosin PL. Segmenting periodic reliefs on triangle meshes. Lecture notes in computer science, vol. 4647. 2007. p. 290–306.
[9] Pauly M, Mitra NJ, Wallner J, Pottmann H, Guibas L. Discovering structural regularity in 3D geometry. ACM Transaction on Graphics 2008;27(3):43.
[10] Bokeloh M, Berner A, Wand M, Seidel HP, Schilling A. Symmetry detection using feature lines. Computer Graphics Forum 2009;28(2):697–706.
[11] Zheng Q, Sharf A, Wan G, Li Y, Mitra NJ, Cohen-Or D, Chen B. Non-local scan consolidation for 3D urban scenes. ACM Transaction on Graphics 2010;29(4):94.
[12] Li M, Langbein FC, Martin RR. Detecting approximate symmetries of discrete point subsets. Computer-Aided Design 2008;40(1):76–93.
[13] Li M, Langbein FC, Martin RR. Detecting design intent in approximate CAD models using symmetry. Computer-Aided Design 2010;42(3):183–201.
[14] Katz S, Tal A. Hierarchical mesh decomposition using fuzzy clustering and cuts. ACM Transactions on Graphics 2003;22(3):954–61.
[15] Katz S, Leifman G, Tal A. Mesh segmentation using feature point and core extraction. The Visual Computer 2005;21(8–10):649–58.
[16] Shammaa HM, Suzuki H, Michikawa T. Registration of CAD mesh models with CT volumetric model of assembly of machine parts. The Visual Computer 2007;23(12):965–74.
[17] Shammaa HM, Suzuki H, Ohtake Y. Extraction of isosurfaces from multi-material CT volumetric data of mechanical parts. In: Proc. ACM symposium on solid and physical modeling. 2008. p. 213–20.
[18] Mizoguchi T, Date H, Kanai S, Kishinami T. Quasi-optimal mesh segmentation via region growing/merging. In: Proc. ASME/DETC. 2007. p. 35171.
[19] Vieira M, Shimada K. Surface mesh segmentation and smooth surface extraction through region growing. Computer-Aided Geometric Design 2005;22(8):771–92.
[20] Besl P, McKay N. A method for registration of 3-D shapes. IEEE Transactions on Pattern Analysis and Machine Intelligence 1992;14(2):239–56.
[21] Kondo D, Mizoguchi T, Kanai S. Recognizing periodicities on 3D scanned meshes based on indexed-ICP algorithm. In: Advances in integrated design and manufacturing in mechanical engineering III. Springer; 2011.
[22] Lorensen WE, Harvey EC. Marching cubes: a high resolution 3D surface construction algorithm. ACM SIGGRAPH Computer Graphics 1987;21(4):163–9.
[23] Geomagic, http://www.geomagic.com.
[24] Mitra NJ, Yang YL, Yan DM, Li W, Agrawala M. Illustrating how mechanical assemblies work. ACM Transaction of Graphics 2010;29(4). Article No. 58.